Resolving the structure of QSO disks through microlensing effects

P. Abolmasov and N. I. Shakura

Black Hole Universe – 2012

Strong lensing and microlensing

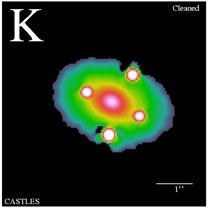

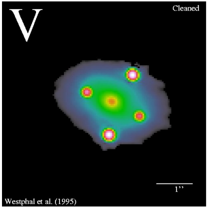

Einstein-Chwolson radius:

$$\theta_{Ein} = \sqrt{\frac{4GM_L}{c^2}\frac{D_{LS}}{D_S D_L}} \simeq 2.8 \times \sqrt{\frac{M}{\mathrm{M}_\odot}\frac{D_{LS}}{D_L}\frac{1\mathrm{Gpc}}{D_S}}\mu\mathrm{as} \tag{1}$$

Strong lensing and microlensing

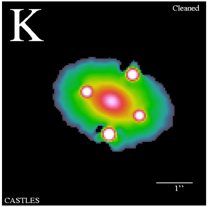

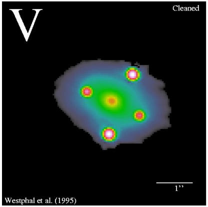

Einstein-Chwolson radius:

$$\theta_{Ein} = \sqrt{\frac{4GM_L}{c^2}\frac{D_{LS}}{D_S D_L}} \begin{array}{ll} \sim \mathrm{mas} & \text{microlensing in our Galaxy} \\ \sim \mathrm{arcsec} & \text{strong lensing} \\ \sim 10\mathrm{arcsec} & \text{galaxy clusters} \\ \sim \mu\mathrm{as} & \text{microlensing at cosmological scales} \end{array} \quad (1)$$

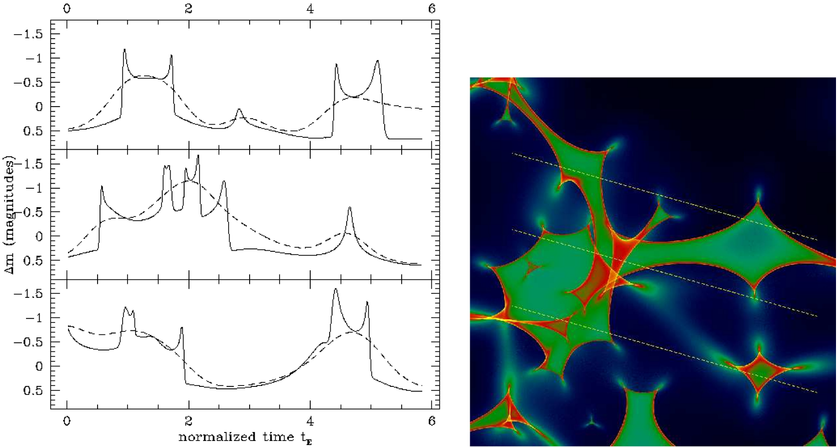

Fig. 45. Microlensing lightcurves for the three tracks shown in Fig. 44. The solid line correspond to a small source (Gaussian shape with width of about 3% of the Einstein radius), the dashed line represents a source that is a factor of 10 larger

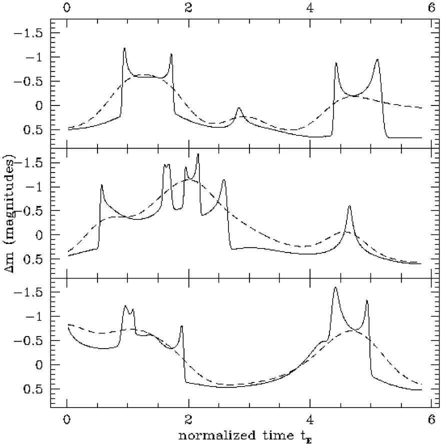

Fig. 45. Microlensing lightcurves for the three tracks shown in Fig. 44. The solid line correspond to a small source (Gaussian shape with width of about 3% of the Einstein radius), the dashed line represents a source that is a factor of 10 larger

half-light radius:

$$\frac{\int_0^{R_{1/2}} I(R)RdR}{\int_0^{+\infty} I(R)RdR} = \frac{1}{2}$$

Standard disk accretion (Shakura & Sunyaev, 1973)

Bolometric flux

$$Q = \frac{3}{8\pi}\frac{GM\dot{M}}{R^3}\left(1-\sqrt{\frac{R_{in}}{R}}\right)$$

Multi-blackbody approximation:

$$I_\nu(r,\nu) = \frac{2h\nu^3}{c^2}\frac{1}{\exp\left(\frac{h\nu}{kT(R)}\right)-1}$$

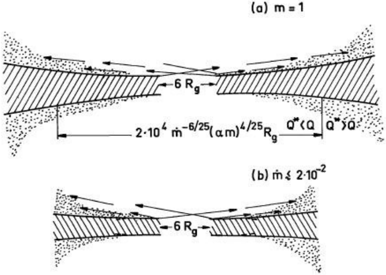

Fig. 4. The thickness of the disk as a function of the distance to the black hole: a) $\dot{M} = \dot{M}_{cr}$. b) $\dot{M} < 10^{-2}\dot{M}_{cr}$. In the central zone, $R < 3R_g$ newtonian mechanics is not applicable. Trajectories of X-ray and ultra-violet quanta which lead to evaporation and heating of the matter in the outer regions of the disk are shown by the arrows. The corona formed by the hot, evaporated matter is denoted by dots

Monochromatic flux from the entire disc:

$$F_\nu = \int I_{\nu,obs}\, d\Omega = \frac{2\pi}{D^2\times(1+z)^3}\cos i \times \int I_{\nu,em}\left(\nu/(1+z)\right) R dR$$

Standard disk accretion (Shakura & Sunyaev, 1973)

Bolometric flux

$$\sigma T^4 = \frac{3}{8\pi} \frac{GM\dot{M}}{R^3} \left(1 - \sqrt{\frac{R_{in}}{R}} \right)$$

Multi-blackbody approximation:

$$I_\nu(r,\nu) = \frac{2h\nu^3}{c^2} \frac{1}{\exp\left(\frac{h\nu}{kT(R)}\right) - 1}$$

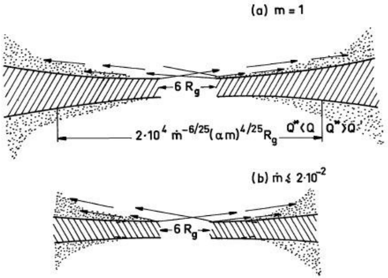

Fig. 4. The thickness of the disk as a function of the distance to the black hole: a) $\dot{M} = \dot{M}_{cr}$. b) $\dot{M} < 10^{-2} \dot{M}_{cr}$. In the central zone, $R < 3R_g$ newtonian mechanics is not applicable. Trajectories of X-ray and ultra-violet quanta which lead to evaporation and heating of the matter in the outer regions of the disk are shown by the arrows. The corona formed by the hot, evaporated matter is denoted by dots

Monochromatic flux from the entire disc:

$$F_\nu = \int I_{\nu,obs} d\Omega = \frac{2\pi}{D^2 \times (1+z)^3} \cos i \times \int I_{\nu,em} \left(\nu/(1+z)\right) R dR$$

Standard disk accretion

Half-light radius:

$$\frac{\int_{R_{in}}^{R_{1/2}} \left(\exp\left(\frac{h\nu_{em}}{kT(R)}\right) - 1\right)^{-1} RdR}{\int_{R_{in}}^{+\infty} \left(\exp\left(\frac{h\nu_{em}}{kT(R)}\right) - 1\right)^{-1} RdR} = \frac{1}{2}$$

neglecting the inner edge: $R_{1/2} \simeq 2.44 R_d$, где $h\nu_{em} = kT(R_d)$

$$R_{1/2} \simeq 2.44 R_d \simeq 2.44 \left(\frac{45 G \lambda_{em}^4 M \dot{M}}{16\pi^6 hc^2}\right)^{1/3} = 2.44 \left(\frac{45 c^3 \lambda_{em}^4 \dot{m}}{4\pi^5 h \varkappa GM}\right)^{1/3} \frac{GM}{c^2} \tag{2}$$

Standard disk accretion

Half-light radius:

$$\frac{\int_{R_{in}}^{R_{1/2}} \left(\exp\left(\frac{h\nu_{em}}{kT(R)}\right)-1\right)^{-1} RdR}{\int_{R_{in}}^{+\infty} \left(\exp\left(\frac{h\nu_{em}}{kT(R)}\right)-1\right)^{-1} RdR} = \frac{1}{2}$$

neglecting the inner edge: $R_{1/2} \simeq 2.44 R_d$, где $h\nu_{em} = kT(R_d)$

$$R_{1/2} \simeq 24.9 \left(\frac{\lambda_{em}}{0.25\mu}\right)^{4/3} \left(\frac{M}{10^9\ \mathrm{M}_\odot}\right)^{-1/3} \dot{m} \times \frac{GM}{c^2} \tag{2}$$

Standard disk accretion

Half-light radius:

$$\frac{\int_{R_{in}}^{R_{1/2}} \left(\exp\left(\frac{h\nu_{em}}{kT(R)}\right)-1\right)^{-1} RdR}{\int_{R_{in}}^{+\infty} \left(\exp\left(\frac{h\nu_{em}}{kT(R)}\right)-1\right)^{-1} RdR} = \frac{1}{2}$$

neglecting the inner edge: $R_{1/2} \simeq 2.44 R_d$, где $h\nu_{em} = kT(R_d)$

$$R_{1/2} \simeq 24.9 \left(\frac{\lambda_{em}}{0.25\mu}\right)^{4/3} \left(\frac{M}{10^9\ \mathrm{M}_\odot}\right)^{-1/3} \dot{m} \times \frac{GM}{c^2} \qquad (2)$$

A more general case:

$$R \propto \lambda^\zeta \qquad (3)$$

- $\zeta = 4/3$ for standard disk
- $\zeta \sim 2$ slim disk, strong irradiation usw.
- $\zeta \to 0$ for a star with no limb-darkening
- $\zeta = 8/7$ for a disk with a strong torque at the inner boundary (Agol & Krolik, 2000)

The challenge of large radii

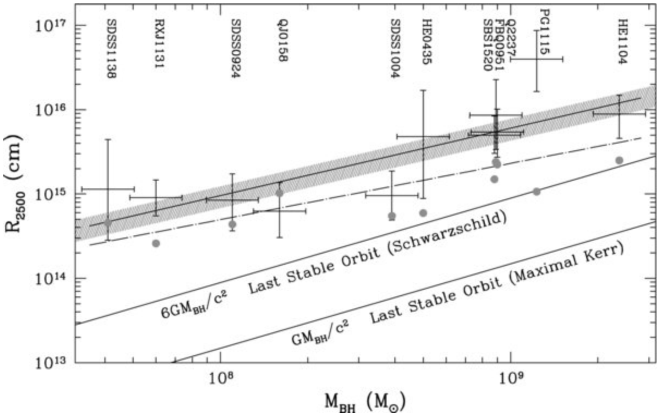

Morgan et al. (2010)

Dependence on wavelength: Blackburne et al. (2011)

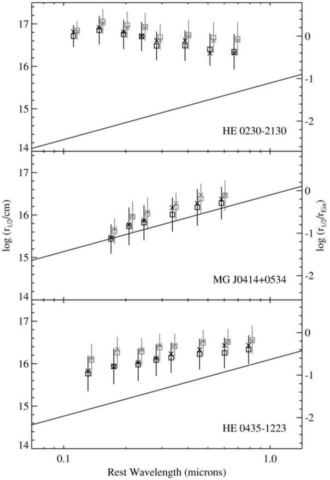

HE0230: $z = 2.162$, $M \simeq 9 \times 10^7\ \mathrm{M}_\odot$

MG0414: $z = 2.64$, $M \simeq 1.8 \times 10^9\ \mathrm{M}_\odot$, radioloud

HE 0435: $z = 1.689$, $M \simeq 5 \times 10^8\ \mathrm{M}_\odot$

Structure parameter versus mass

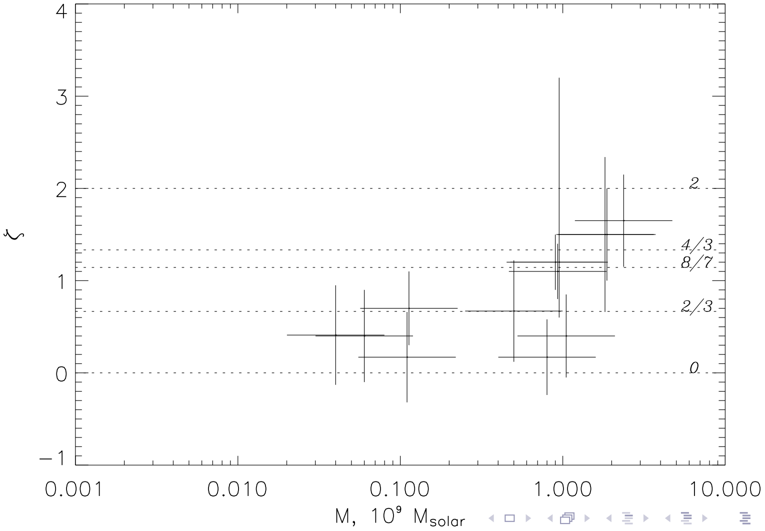

Summarizing the observational material

- massive black holes ($M \gtrsim 10^9\ \mathrm{M}_\odot$) have nearly standard disks
- smaller black hole masses conform less with the standard model
- "disk" size is practically independent on wavelength for smaller-mass quasars
- there is no evidence for strong spectral energy distribution variations among quasar populations (blue bump works well)

Summarizing the observational material

- massive black holes ($M \gtrsim 10^9\ \mathrm{M}_\odot$) have nearly standard disks
- smaller black hole masses conform less with the standard model
- "disk" size is practically independent on wavelength for smaller-mass quasars
- there is no evidence for strong spectral energy distribution variations among quasar populations (blue bump works well)

- bright quasars accrete at several Solar masses per year that makes lighter black holes super-Eddington accretors
- supercritical accretors form hot outflows that manifest themselves though electron scattering

Lampshade model

Same flux, same broad-band spectrum, but different spatial properties

Supercritical disk outflows

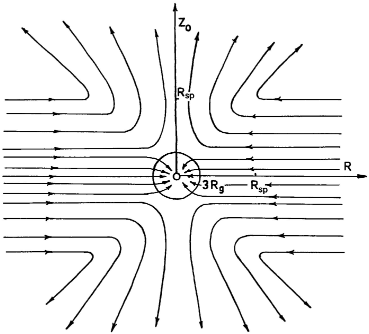

Fig. 8. Lines of matter flow at supercritical accretion (the disk section along the Z-coordinate). When $R < R_{sp}$ spherization of accretion takes place and the outflow of matter from the collapsar begins

Shakura & Sunyaev (1973)

Supercritical disk outflows

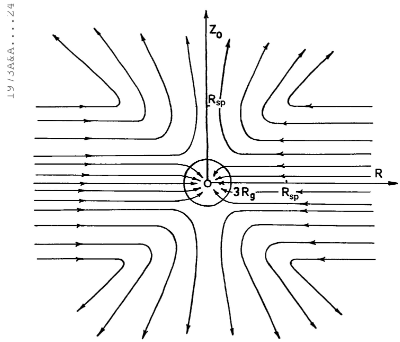

Fig. 8. Lines of matter flow at supercritical accretion (the disk section along the Z-coordinate). When $R < R_{sp}$ spherization of accretion takes place and the outflow of matter from the collapsar begins

Shakura & Sunyaev (1973)

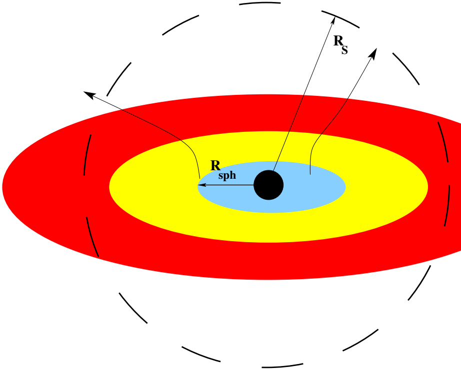

Condition for an outflow

Natural normalization for accretion rate

$$\dot{M}^* = \frac{4\pi GM}{c\varkappa} \tag{4}$$

Critical rate: $\dot{M}_{cr} = \dot{M}^*/\eta$. Mass accretion rate $\dot{M} = \dot{M}^* \dot{m}$.

Condition for an outflow

Natural normalization for accretion rate

$$\dot{M}^* = \frac{4\pi GM}{c\varkappa} \tag{4}$$

Critical rate: $\dot{M}_{cr} = \dot{M}^*/\eta$. Mass accretion rate $\dot{M} = \dot{M}^* \dot{m}$.
Radiation pressure overcomes gravity...

Condition for an outflow

Natural normalization for accretion rate

$$\dot{M}^* = \frac{4\pi GM}{c\varkappa} \tag{4}$$

Critical rate: $\dot{M}_{cr} = \dot{M}^*/\eta$. Mass accretion rate $\dot{M} = \dot{M}^* \dot{m}$.
Radiation pressure overcomes gravity...

$$\frac{\varkappa F}{c} > \frac{GMz}{(R^2 + z^2)^{3/2}}$$

Condition for an outflow

Natural normalization for accretion rate

$$\dot{M}^* = \frac{4\pi GM}{c\varkappa} \tag{4}$$

Critical rate: $\dot{M}_{cr} = \dot{M}^*/\eta$. Mass accretion rate $\dot{M} = \dot{M}^*\dot{m}$.
Radiation pressure overcomes gravity...

$$\frac{\varkappa}{c}\frac{3}{8\pi}\frac{GM\dot{M}}{R^3}\left(1-\sqrt{\frac{R_{in}}{R}}\right) > \frac{GMz}{(R^2+z^2)^{3/2}} \simeq \frac{GM}{R^2}$$

$$\frac{r}{1-1/\sqrt{r}} = \frac{3}{2}\frac{\dot{m}}{x_{in}} \qquad R = R_{in}r = \frac{GM}{c^2}\times x_{in}\times r$$

Condition for an outflow

Natural normalization for accretion rate

$$\dot{M}^* = \frac{4\pi GM}{c\varkappa} \tag{4}$$

Critical rate: $\dot{M}_{cr} = \dot{M}^*/\eta$. Mass accretion rate $\dot{M} = \dot{M}^*\dot{m}$.
Radiation pressure overcomes gravity...

$$\frac{\varkappa}{c}\frac{3}{8\pi}\frac{GM\dot{M}}{R^3}\left(1-\sqrt{\frac{R_{in}}{R}}\right) > \frac{GMz}{(R^2+z^2)^{3/2}} \simeq \frac{GM}{R^2}$$

$$\frac{r}{1-1/\sqrt{r}} = \frac{3}{2}\frac{\dot{m}}{x_{in}} \qquad R = R_{in}r = \frac{GM}{c^2}\times x_{in}\times r$$

First contact at $r = 9/4$, supercritical regime at $\dot{m} > \frac{9}{2}x_{in}$
Spherization radius obtained as a solution of a cubic equation for $\sqrt{r}$.

Spherization radius:

$$R_{sph} = \frac{GM}{c^2}\dot{m} \times \cos^2\left(\frac{1}{3}\arccos\left(-3\sqrt{\frac{2x_{in}}{\dot{m}}}\right)\right) \quad (5)$$

For $\dot{m} \gg 1$, the cosine $\to \cos(\pi/6) = \sqrt{3}/2$, hence:

$$R_{sph} \simeq \frac{3}{2}\dot{m} \times \frac{GM}{c^2}$$

Envelope radius

Continuity condition for $v_R = const$:

$$f_w \dot{M} = \dot{M}_w = 4\pi R^2 v_w \rho(R)$$

Envelope radius

Radial optical depth:

$$\tau(R) = \int_R^{+\infty} \varkappa \rho(R) dR = \frac{\varkappa \dot{M}_w}{v_w} \frac{1}{R}$$

Envelope radius

Radial optical depth:

$$\tau(R) = \int_R^{+\infty} \varkappa\rho(R)dR = \frac{\varkappa\dot{M}_w}{v_w}\frac{1}{R}$$

Here, $v_w = \sqrt{2GM/R_w}$ is wind velocity, $R_w \simeq R_{sph}$. Mass loss rate $\dot{M}_w = f_w\dot{M}$.

Envelope radius

Radial optical depth:

$$\tau(R) = \int_R^{+\infty} \varkappa \rho(R) dR = \frac{\varkappa \dot{M}_w}{v_w} \frac{1}{R}$$

Here, $v_w = \sqrt{2GM/R_w}$ is wind velocity, $R_w \simeq R_{sph}$. Mass loss rate $\dot{M}_w = f_w \dot{M}$. Radius $R_1 = R(\tau = 1)$:

$$R_1 \simeq \frac{\varkappa \dot{M}_w}{4\pi} \times \sqrt{\frac{R_{sph}}{2GM}}$$

$$\frac{R_1 c^2}{GM} = \frac{f_w}{\sqrt{2}} \dot{m}^{3/2} \times \cos\left(\frac{1}{3}\arccos\left(-3\sqrt{\frac{2x_{in}}{\dot{m}}}\right)\right) \quad (6)$$

Envelope radius

Radial optical depth:

$$\tau(R) = \int_R^{+\infty} \varkappa \rho(R) dR = \frac{\varkappa \dot{M}_w}{v_w} \frac{1}{R}$$

Here, $v_w = \sqrt{2GM/R_w}$ is wind velocity, $R_w \simeq R_{sph}$. Mass loss rate $\dot{M}_w = f_w \dot{M}$. Radius $R_1 = R(\tau = 1)$:

$$R_1 \simeq \frac{\varkappa \dot{M}_w}{4\pi} \times \sqrt{\frac{R_{sph}}{2GM}}$$

$$\frac{R_1 c^2}{GM} = \frac{f_w}{\sqrt{2}} \dot{m}^{3/2} \times \cos\left(\frac{1}{3} \arccos\left(-3\sqrt{\frac{2x_{in}}{\dot{m}}}\right)\right) \qquad (6)$$

Total optical depth R_d: $\tau \sim R_1/R_d$

Three cases:

- subcritical
- supercritical, $R_d \gtrsim R_1$ – accretion disc directly visible
- supercritical, $R_d \lesssim R_1$ – optically thick photosphere

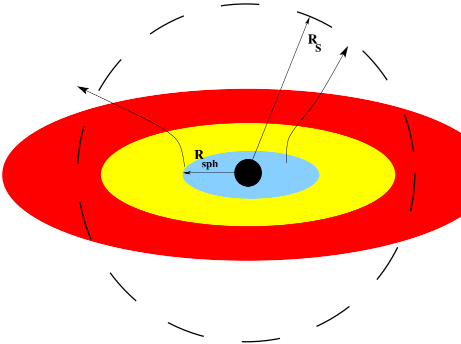

Three cases:

- subcritical
- supercritical, $R_d \gtrsim R_1$ – accretion disc directly visible
- supercritical, $R_d \lesssim R_1$ – optically thick photosphere

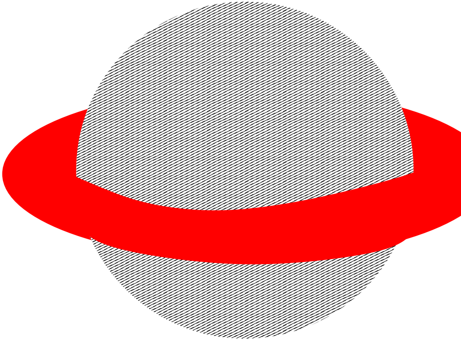

Three cases:

- subcritical
- supercritical, $R_d \gtrsim R_1$ – accretion disc directly visible
- supercritical, $R_d \lesssim R_1$ – optically thick photosphere

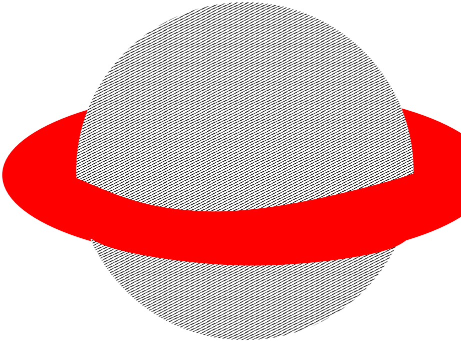

Standard disk flux

$$F_\nu \simeq 6.9 \cos i\, \dot{m}^{2/3} \left(\frac{\lambda_{obs}}{1\mu}\right)^{-1/3} \left(\frac{M}{10^9\ \mathrm{M}_\odot}\right)^{4/3} \times \left(\frac{D}{1\mathrm{Gpc}}\right)^{-2} (1+z)^{-8/3}\ \mathrm{mJy}$$

Standard disk flux

$$F_\nu \simeq 6.9 \cos i \, \dot{m}^{2/3} \left(\frac{\lambda_{obs}}{1\mu}\right)^{-1/3} \left(\frac{M}{10^9\ \mathrm{M}_\odot}\right)^{4/3} \times \left(\frac{D}{1\mathrm{Gpc}}\right)^{-2} (1+z)^{-8/3}\ \mathrm{mJy}$$

(normalization for F814W *HST* data) =>

$$M \simeq 4.5 \times 10^7 \left(\frac{D}{1\mathrm{Gpc}}\right)^{3/2} (1+z)^2 \times \dot{m}^{-1/2} \times 10^{-0.3(I-19)}\ \mathrm{M}_\odot \quad (7)$$

$\dot{m}$ -?

Standard disk flux

$$F_\nu \simeq 6.9 \cos i\, \dot{m}^{2/3} \left(\frac{\lambda_{obs}}{1\mu}\right)^{-1/3} \left(\frac{M}{10^9\ \mathrm{M}_\odot}\right)^{4/3} \times \left(\frac{D}{1\mathrm{Gpc}}\right)^{-2} (1{+}z)^{-8/3}\ \mathrm{mJy}$$

(normalization for F814W *HST* data) =>

$$M \simeq 4.5 \times 10^7 \left(\frac{D}{1\mathrm{Gpc}}\right)^{3/2} (1+z)^2 \times \dot{m}^{-1/2} \times 10^{-0.3(I-19)}\ \mathrm{M}_\odot \quad (7)$$

$\dot{m}$ -? $M^2\dot{m}$ is measured from flux

Standard disk flux

$$F_\nu \simeq 6.9 \cos i\, \dot{m}^{2/3} \left(\frac{\lambda_{obs}}{1\mu}\right)^{-1/3} \left(\frac{M}{10^9\ \mathrm{M}_\odot}\right)^{4/3} \times \left(\frac{D}{1\mathrm{Gpc}}\right)^{-2} (1+z)^{-8/3}\ \mathrm{mJy}$$

(normalization for F814W *HST* data) =>

$$M \simeq 4.5 \times 10^7 \left(\frac{D}{1\mathrm{Gpc}}\right)^{3/2} (1+z)^2 \times \dot{m}^{-1/2} \times 10^{-0.3(I-19)}\ \mathrm{M}_\odot \quad (7)$$

$\dot{m}$ -? $M^2\dot{m}$ is measured from flux
No new information from radius estimates in the standard disc model!

$$R_{1/2} \propto (M^2 \dot{m})^{1/3},$$

$\dot{m}$ and mass estimates: standard disk behind a scattering envelope

$$R_\mu \simeq 1.6 R_1$$

$$\frac{R_1 c^2}{GM} = \frac{f_w}{\sqrt{2}} \dot{m}^{3/2} \times \cos\left(\frac{1}{3}\arccos\left(-3\sqrt{\frac{2x_{in}}{\dot{m}}}\right)\right) \tag{8}$$

$$\dot{m} \simeq 137 \left(\frac{\lambda_{obs}}{1\mu}\right)^{-1/4} \times 10^{0.3(I-19)} \times \left(\frac{D}{1\mathrm{Gpc}}\right)^{-3/4} \times \\ \times (1+z)^{-2} \times \frac{R_1}{10^{15}\mathrm{cm}} \frac{1}{\cos\left(\frac{1}{3}\arccos\left(-3\sqrt{\frac{2x_{in}}{\dot{m}}}\right)\right)} \tag{9}$$

accretion rate is found by simple iteration

$\dot{m}$ and mass estimates: results

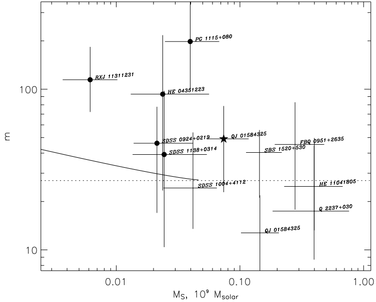

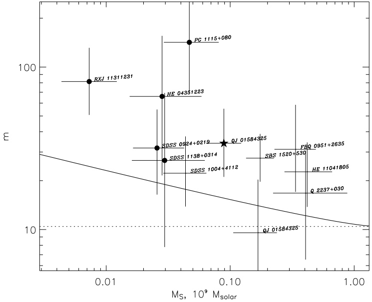

$a = 0 \;=>\; x_{in} = 6$ $\qquad$ $a = 0.9 => x_{in} \simeq 2.3$

Accretion is subcritical below the dotted line

Disk size is larger than the envelope size behind the solid line (for $\lambda = 0.25\mu\mathrm{m}$, $R_{1/2}$ are compared)

Physical $\dot{M}$ and masses

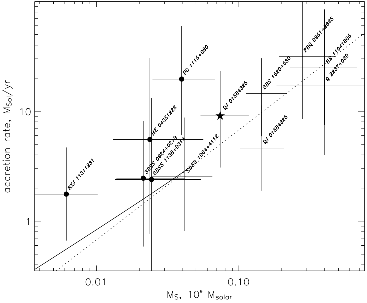

$a = 0 \ \ => x_{in} = 6$

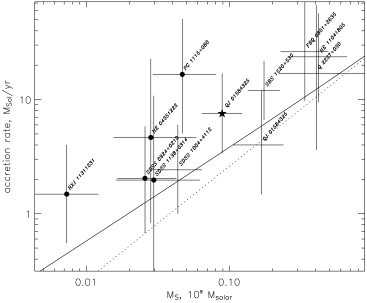

$a = 0.9 => x_{in} \simeq 2.3$

Photometrical evidence for supercritical QSO

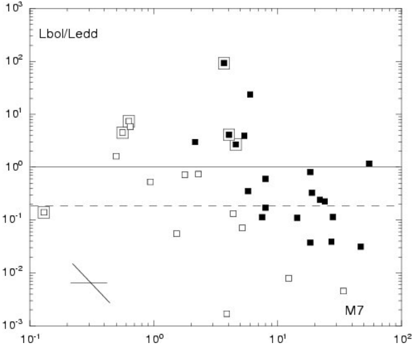

Collin et al. (2002)
solid and dashed line are Eddington limits for $a = 0$ and $a \to 1$
absorption-line QSO objects with slow outflows are shown by large squares

Spectral evidence for outflows: UV range

$$v/c \sim \dot{m}^{-1/2} \sim 0.02..0.3$$

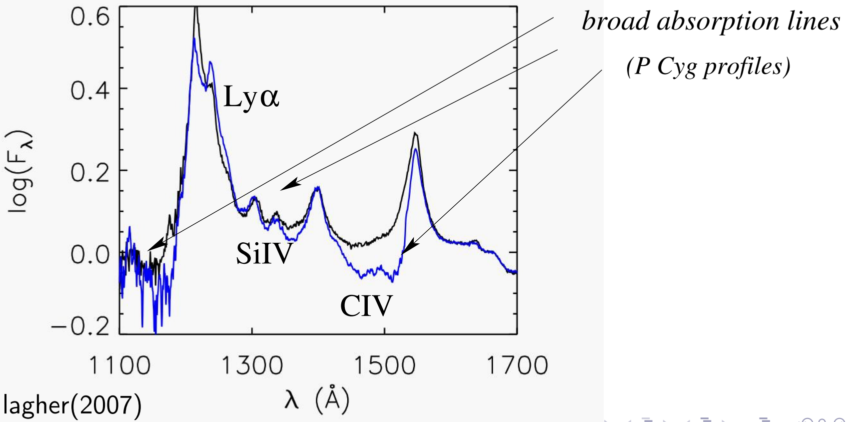

Gallagher(2007)

Spectral evidence for outflows: X-rays

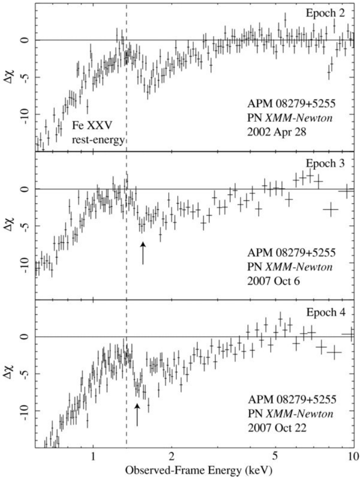

Chartas et al. (2009)

$\Delta\chi$ residuals between the best-fit Galactic absorption and power-law model and the XMM-Newton pn spectra of APM 08279+5255

Source sizes in X-rays

$$R_X \sim \text{ several } \times \frac{GM}{c^2}$$

for both super- (HE 0435-1223, see Blackburne et al. (2011)) and sub-Eddington (QSO J2237+0305, see Chen et al. (2011); Q J0158-4325, see Morgan et al. (2012)) sources

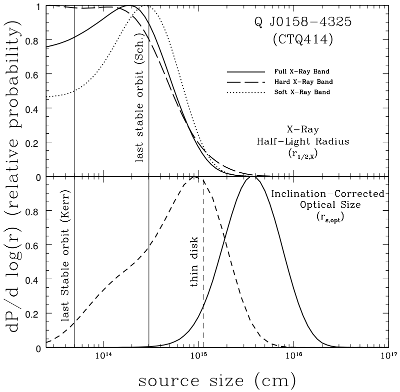

High-amplification events

$\mu \propto \Delta t^{-1/2}$

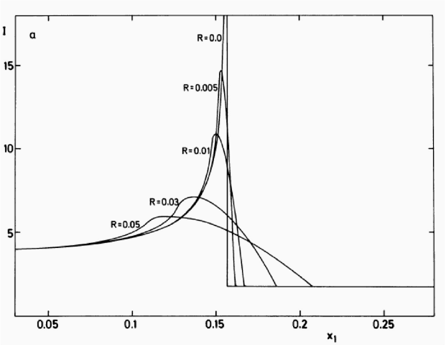

Microlensing of an inclined relativistic disc

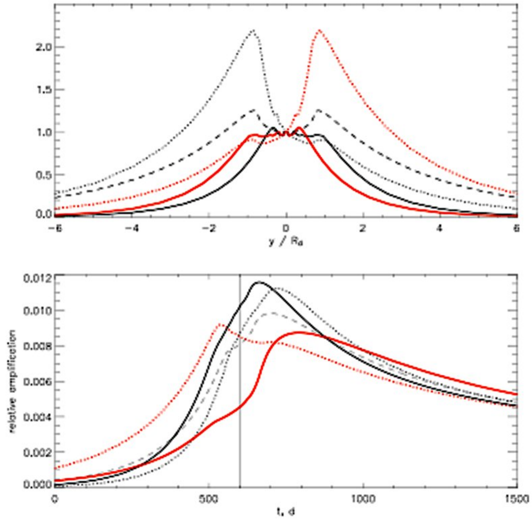

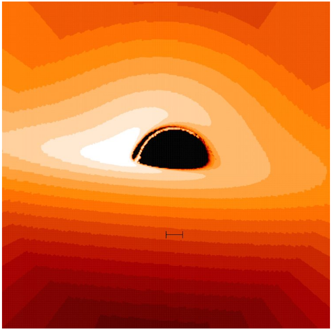

dashed line – without relativistic effects

QSO J2237+0305 image A

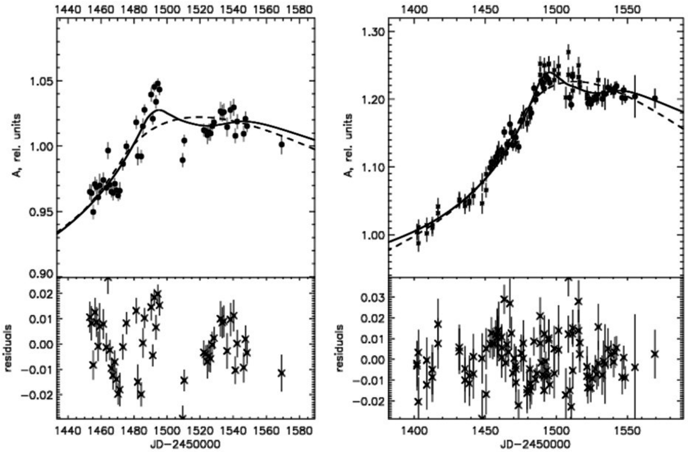

$a = 0.2^{0.8}_{-0.7}$, $M = 4^{+5}_{-3}$, $i = 70 \pm 10\,\mathrm{deg}$, $\psi = 100 \pm 15\,\mathrm{deg}$, $\mu_1/\mu_0 = 0.6..1.1$

QSO J2237+0305 image C

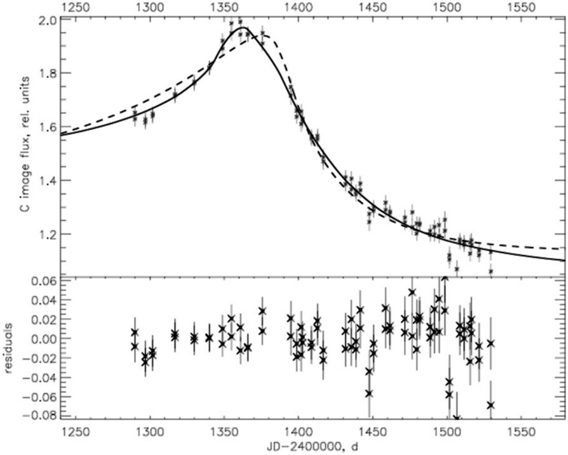

$a = 0.97 \pm 0.02$
$M = 1^{+1}_{-0.3} \times 10^{10}\ \mathrm{M}_{\odot}$
$i = 85 \pm 5$ deg
$\psi = 53 \pm 10$ deg
$\mu_1/\mu_0 = 2.09 \pm 0.05$
$\chi^2/DOF = 88/75$

Conclusions:

- considerable part of high-redshift quasars are accreting in moderately super-Eddington regime
- supercritical disk envelope allows self-consistent mass estimates in microlensed quasars
- BAL quasars may be linked with super-Eddington sources
- inner parts of the disk (several GM/c^2) are visible and emit X-rays
- inner disk structure may be traced through the fine structure of high-amplification events

Thank you for attention!

Agol E., Krolik J. H., 2000, ApJ, 528, 161

Blackburne J. A., Kochanek C. S., Chen B., Dai X., Chartas G., 2011, ArXiv e-prints

Blackburne J. A., Pooley D., Rappaport S., Schechter P. L., 2011, ApJ, 729, 34

Chartas G., Saez C., Brandt W. N., Giustini M., Garmire G. P., 2009, ApJ, 706, 644

Chen B., Dai X., Kochanek C. S., Chartas G., Blackburne J. A., Kozlowski S., 2011, ArXiv e-prints

Collin S., Boisson C., Mouchet M., Dumont A.-M., Coupé S., Porquet D., Rokaki E., 2002, A&A, 388, 771

Morgan C. W., Hainline L. J., Chen B., Tewes M., Kochanek C. S., Dai X., Kozlowski S., Blackburne J. A., Mosquera A. M., Chartas G., Courbin F., Meylan G., 2012, ArXiv e-prints

Morgan C. W., Kochanek C. S., Morgan N. D., Falco E. E., 2010, ApJ, 712, 1129

Pooley D., Blackburne J. A., Rappaport S., Schechter P. L., 2007, ApJ, 661, 19

Shakura N. I., Sunyaev R. A., 1973, A&A, 24, 337